NISTIR 89-3909

CLUTTER MODELS FOR SUBSURFACE ELECTROMAGNETIC APPLICATIONS

David A. Hill

National Institute of Standards and Technology
(formerly National Bureau of Standards)
U.S. Department of Commerce
Boulder, Colorado 80303-3328

February 1989

NISTIR 89-3909

CLUTTER MODELS FOR SUBSURFACE ELECTROMAGNETIC APPLICATIONS

David A. Hill

Electromagnetic Fields Division
Center for Electronics and Electrical Engineering
National Engineering Laboratory
National Institute of Standards and Technology
(formerly National Bureau of Standards)
Boulder, Colorado 80303-3328

February 1989

Sponsored by
U.S. Army Belvoir RD&E Center
Fort Belvoir, VA 22060

U.S. DEPARTMENT OF COMMERCE, Robert A. Mosbacher, Secretary
Ernest Ambler, Acting Under Secretary for Technology
NATIONAL INSTITUTE OF STANDARDS AND TECHNOLOGY, Raymond G. Kammer, Acting Director

CONTENTS

CLUTTER MODELS FOR SUBSURFACE ELECTROMAGNETIC APPLICATIONS

David A. Hill

Electromagnetic Fields Division
National Institute of Standards and Technology
Boulder, CO 80303

Clutter models for subsurface electromagnetic applications are discussed with emphasis on tunnel detection applications. Random medium models are more versatile and require less detailed information than deterministic models. The Born approximation is used to derive expressions for the incoherent field, and electric and magnetic dipoles are treated in detail. When random inhomogeneities are located in the near field of the dipole source, an electric dipole radiates a larger incoherent field than a magnetic dipole because of its larger reactive electric field.

Key words: clutter; coherent field; electric dipole; incoherent field; magnetic dipole; random medium.

1. INTRODUCTION

The use of electromagnetic (EM) waves in subsurface applications continues to increase. Some current applications are geophysical prospecting [1-3], mine communication [4,5], tunnel detection [6-8], and mine detection [9,10]. The simplest earth model is a homogeneous medium; a horizontally stratified medium [11,12] is a better earth model for some applications [13-16].

EM transmission measurements for tunnel detection [7] and scattering measurements for remote sensing [17] indicate that the real earth is often inhomogeneous in a fairly complicated manner. When an EM wave propagates through an inhomogeneous medium, it suffers attenuation and dispersion, and an incoherent (clutter) signal is produced by scattering. Such effects are detrimental to tunnel detection [7], but they have not been quantitatively evaluated. In some applications of geophysical tomography [18-19], random noise has been added to the received signal to test the sensitivity of the imaging algorithm. Such tests are useful, but it would be more realistic if

we had mathematical models for clutter signals that represent the physics of an inhomogeneous earth.

A typical borehole-to-borehole example for tunnel detection is shown in figure 1. The received signal is made up of a direct-path signal, a signal scattered from the target (in this case a tunnel), and a clutter signal scattered from the inhomogeneities in the rock. In typical analyses of EM detection of tunnels [20,21], the clutter signal is not included. However, the clutter signal (sometimes called geologic noise [22]) is often the main limitation in tunnel detection. In underground communication or source location [23], the target signal does not exist, but the direct-path signal is still contaminated with the clutter signal. This report is primarily concerned with clutter models for use in the analysis of tunnel detection and other subsurface applications.

The organization of this report is as follows. Section 2 discusses types of inhomogeneous earth models, both deterministic and random. Random media models offer more flexibility, and the mathematical techniques for analyzing random media are discussed in section 3. The analysis of an electric dipole radiating in a random medium is contained in section 4. Numerical results are given for both the far-field pattern and the total radiated incoherent power. Analogous results are given for a magnetic dipole source in section 5. Section 6 contains an analysis for transmission between electric dipoles for both cw and pulse excitation. Conclusions and recommendations for further work are contained in section 7.

2. INHOMOGENEOUS EARTH MODELS

In this section, we discuss three types of inhomogeneous earth models. Deterministic models are useful when the details of the local earth medium are well known, but they require more information than is generally available for most applications. Random media models are more flexible and require less information. However, the EM fields propagating in random media are random variables, and they can be described only statistically.

2.1 Deterministic Models

The most useful deterministic model is composed of a homogeneous earth with a single scatterer whose response can be calculated. In this case the scattered field is considered to be the clutter signal. For example in the problem of surface location of a buried magnetic dipole source, location errors caused by scattering from a sphere [23] or a prolate spheroid [24] have been evaluated. The geologic noise caused by a more complicated overburden scatterer in geophysical prospecting has been evaluated numerically [22].

In these cases the parameters that describe the scatterer (dimensions, location, constitutive parameters, etc.) are deterministic quantities, and the scattered fields are deterministic. Thus the scatterer parameters are chosen from a knowledge of the specific application, and each case yields only one deterministic result for the clutter signal. Repeated calculations for different parameters are required for general clutter characteristics, and such repeated calculations can be tedious. For tunnel detection where the structure of the rock is not well known, we favor random media models because statistical properties of the clutter are obtained directly. Consequently, the remainder of this report will deal with random media models.

2.2 Random Discrete Scatterers

Random media can generally be grouped into three categories [25]: random scatterers, random continua, and rough surfaces. We will not consider rough surfaces in this report because we assume that volume clutter is more important than surface clutter in most tunnel detection applications. However, for cases where the source or receiver is located near the earth surface or near a subsurface layer with a rough boundary, rough surface clutter could be important.

Typical examples of discrete scatterers are rain [26] and hail. Discrete scatterers can be characterized by their bistatic radar cross section $\sigma_{bi}(\hat{o},\hat{i})$, where $\hat{i}$ is a unit vector in the direction of propagation of the incident wave and $\hat{o}$ is the direction of the scattered wave [25, Sec. 2-1]. (Vectors and dyads are indicated by boldface throughout this report.)

For a random, uniform distribution of identical scatterers, the other important parameter is the number ρ of scatterers per unit volume.

For a tenuous distribution of scatterers in the far field of the source, such as a weather radar [26], the single-scattering approximation yields a fairly simple volume integral expression for the scattered power [25, Sec. 4-1]. The cases of a dense distribution or a near-field source are more complicated.

2.3 A Random Continuum

In this report we define a random continuum as a medium whose permittivity is a random continuous function of position. In some cases, such as atmospheric turbulence [27], the permittivity is also considered to be a function of time. In modelling the earth, we assume that the permittivity $\epsilon(\mathbf{r})$ is a random function of position $\mathbf{r}$ only.

We write the earth permittivity as a sum of the average value ϵ_0 and a fluctuation:

$$\epsilon(\mathbf{r}) = \epsilon_0[1 + \epsilon_1(\mathbf{r})], \tag{1}$$

where ϵ_1 is the fluctuation with zero average

$$<\epsilon_1(\mathbf{r})> = 0 \tag{2}$$

and $< >$ represents the ensemble average [28]. For lossless media, ϵ_0 and ϵ_1 are real, but for lossy media we make them complex. If the medium is statistically homogeneous and isotropic, then the covariance $<\epsilon_1(\mathbf{r}_1)\epsilon_1^*(\mathbf{r}_2)>$ is a function only of the difference $r_d = |\mathbf{r}_d| = |\mathbf{r}_1 - \mathbf{r}_2|$:

$$<\epsilon_1(\mathbf{r}_1)\epsilon_1^*(\mathbf{r}_2)> = B_\epsilon(r_d), \tag{3}$$

where superscript * denotes complex conjugate.

The equivalence between continuous and discrete scattering models has been studied by Besieris [29]. As we will see in section 3, the scattering cross section per unit volume can be written in terms of the Fourier transform of B_ϵ. Various analytical forms of $B_\epsilon(r_d)$ have been used [25, Ch. 16], and anisotropic forms of $B_\epsilon(r_d)$ have been used for anisotropic media such as vegetation [30,31]. In this report we use only the isotropic form $B_\epsilon(r_d)$ because it is simpler, but anisotropic forms might be more realistic for modelling nonspherical inhomogeneities or fractures.

3. MATHEMATICAL METHODS FOR RANDOM MEDIA

An EM wave propagating in a random medium can be expressed as the sum of an average field and a fluctuating field. The average field is also called the coherent field, and the fluctuating field is also called the incoherent field [25, Sec. 4-4]. For example, we can write a scalar component of the total time-harmonic electric field $E_u(\mathbf{r})$ as

$$E_u(r) = \langle E_u(r) \rangle + E_{fu}(r), \tag{4}$$

where $\langle E_u(r) \rangle$ is the average (coherent) field and $E_{fu}(\mathbf{r})$ is the fluctuating (incoherent) field. The time dependence $\exp(-i\omega t)$ is suppressed throughout this report.

3.1 Coherent Field

When an EM wave propagates through a random medium, the average (coherent) field is generally attenuated and slowed by scattering. However, if the randomness is very weak, then the coherent field can be approximated by the incident field that would propagate in a uniform medium. The approximation of the coherent field by the incident field is known as the Born approximation [25, Sec. 4-1].

Karal and Keller [32,33] have used a perturbation technique to study propagation in a random continuum. They have derived a dispersion equation for the effective wavenumber for plane-wave propagation and have derived expressions for the effective dielectric constant and conductivity. Roth and Elachi [34] have used the dispersion equation of Karal and Keller to generate numerical results for loss tangent as a function of the parameters of a random continuum with an exponential correlation function.

When the medium has strong fluctuations, perturbation methods are no longer valid. Dyson's equation for the coherent field [34] is exact in principle, but various approximate methods [34-39] are required to obtain a solution.

3.2 Incoherent Field

By definition the average value of the incoherent field is zero. For example, from (4) we can see that $\langle E_{uf} \rangle = 0$. However, if we take the average of the square of the absolute value of (4), then we can write

$$\langle |E_u|^2 \rangle = |\langle E_u \rangle|^2 + \langle |E_{fu}|^2 \rangle. \tag{5}$$

If we use Ishimaru's terminology [25, Sec. 4-4], then $\langle |E_u|^2 \rangle$ is the average intensity $\langle I \rangle$, $|\langle E_u \rangle|^2$ is the coherent intensity I_c, and $\langle |E_{fu}|^2 \rangle$ is the incoherent intensity I_i. Thus (5) could be written

$$\langle I \rangle = I_c + I_i. \tag{6}$$

Ishimaru's definitions are actually applied to scalar fields, but we can use the same terms for scalar components E_u of the electric field or the vector field **E**. If we want the intensities to have units of W/m^2, then each term in (5) or (6) should be multiplied by the intrinsic impedance η_0 of the

medium. In most cases we will be interested in the ratio I_i/I_c, and the intrinsic impedance will cancel out.

In a weakly random medium, the coherent intensity is nearly the same as the intensity in absence of randomness, and the incoherent intensity I_i can be considered the intensity of the clutter signal. Thus the main problem in clutter applications is the evaluation of the incoherent intensity $I_i = \langle |E_{fu}|^2 \rangle$. The simplest methods for calculating I_i use the Born approximation [25, Sec. 2-6], and we will use the Born approximation throughout the remainder of this report. There are more sophisticated methods, such as the Bethe-Salpeter equation [25], for calculating I_i, but the earth medium has not been well characterized in tunnel detection, and there is no point in making the initial calculations overly complicated.

We can start the analysis by writing the source-free wave equation for the electric field **E**,

$$\nabla \times \nabla \times \mathbf{E} - \omega^2 \mu_0 \epsilon_0 (1 + \epsilon_1)\mathbf{E} = 0, \tag{7}$$

where μ_0 is the permeability of the medium and the permittivity has been written in the form shown in (1). We now write (7) in the equivalent form,

$$\nabla \times \nabla \times \mathbf{E} - k_0^2 \mathbf{E} = k_0^2 \epsilon_1 \mathbf{E}, \tag{8}$$

where $k_0^2 = \omega^2 \mu_0 \epsilon_0$. We can write the total field **E** as the sum of the incident field $\mathbf{E}_0$ and the scattered field $\mathbf{E}_1$:

$$\mathbf{E} = \mathbf{E}_0 + \mathbf{E}_1. \tag{9}$$

The incident field satisfies

$$\nabla \times \nabla \times E_0 - k_0^2 E_0 = 0. \tag{10}$$

If we subtract (10) from (8), we obtain

$$\nabla \times \nabla \times E_1 - k_0^2 E_1 = k_0^2 \epsilon_1 E. \tag{11}$$

We assume that we know the incident field which satisfies (10). The scattered field E_1 satisfies the wave equation with a source term on the right side as given by (11). The problem is that the source term in (11) is not known because E is not known. In the Born approximation [25, 2-6], we approximate E by the incident field E_0 in the source term in (11). Thus the scattered field approximately satisfies the inhomogeneous wave equation,

$$\nabla \times \nabla \times E_1 - k_0^2 E_1 = k_0^2 \epsilon_1 E_0. \tag{12}$$

Since the right side of (12) is known, we can write E_1 in integral form using the Green's function approach [40]

$$E_1(r) = k_0^2 \int_V \epsilon_1(r')\, G(r,r') \cdot E_0(r')\, dr', \tag{13}$$

where G(r,r') is the dyadic Green's function and the integration volume V is all space. In some remote sensing cases, G(r,r') could be the dyadic Green's function for a layered medium [29,30], but we consider only a homogeneous medium (constant k_0) for the deterministic portion of the problem. In this case, G(r,r') is [40]

$$G(r,r') = \frac{1}{4\pi} \left(1 + \frac{1}{k_0^2} \nabla\nabla\right) \psi, \tag{14}$$

where $\psi = \exp(ik_0|\mathbf{r} - \mathbf{r}'|)/|\mathbf{r} - \mathbf{r}'|$ and $\mathbf{1}$ is the unit dyad. For points where $\mathbf{r} = \mathbf{r}'$, either $\mathbf{G}$ or the integral in (13) must be appropriately modified [41,42]. We can also write (13) in component form for a scalar component E_{1u} of $\mathbf{E}_1$:

$$E_{1u}(\mathbf{r}) = k_0^2 \int_V \epsilon_1(\mathbf{r}')\, G_{uv}(\mathbf{r},\mathbf{r}')\, E_{0v}(\mathbf{r}')\, d\mathbf{r}', \tag{15}$$

where G_{uv} is a scalar component of $\mathbf{G}$ and the repeated subscript v indicates summation over the three values of v. From (15) we can see that $\langle E_{1u}\rangle = 0$ because $\langle\epsilon_1\rangle = 0$.

To evaluate the incoherent intensity, we need to evaluate $\langle|E_{1u}|^2\rangle$. If we multiply (15) by its complex conjugate and take the average value, we obtain

$$\langle|E_{1u}(\mathbf{r})|^2\rangle = |k_0|^4 \int_V \int_V B_\epsilon(|\mathbf{r}' - \mathbf{r}''|)\, G_{uv}(\mathbf{r},\mathbf{r}')E_{0v}(\mathbf{r}')\cdot$$

$$G^*_{uw}(\mathbf{r},\mathbf{r}'')E^*_{0w}(\mathbf{r}'')\, d\mathbf{r}'\, d\mathbf{r}'', \tag{16}$$

where we have used (3) to introduce B_ϵ into (16). In the modified Born approximation [43,44], the Green's function in (16) is replaced by the effective Green's function for the random medium.

Generally the double volume integral in (16) is difficult to evaluate, but when the random volume is in the far field of the source and observer, the integrals simplify considerably [25,27]. For the geometry in figure 2, Ishimaru [25, Sec. 16.1] writes the received power P_r as

$$P_r = P_t \int_V \frac{\lambda^2 G_t(\hat{i}) G_r(\hat{o})}{(4\pi)^2 R_1^2 R_2^2}\, \sigma(\hat{o},\hat{i})\, dV, \tag{17}$$

where P_t is the transmitted power, G_t and G_r are the gains of the transmitting and receiving antennas, R_1 and R_2 are the distances shown in figure 2, V is the volume shown in figure 2, and λ is the wavelength. We assume here that the medium is lossless, but an exponential loss factor can be included when necessary. The bistatic scattering cross section per unit volume $\sigma(\hat{o},\hat{i})$ can be derived in terms of B_ϵ in integral form [25, 16.2]

$$\sigma(\hat{o},\hat{i}) = \pi k_0^4 \sin^2\chi \, \Phi_\epsilon(k_s)/2, \tag{18}$$

where $\Phi_\epsilon(K) = \frac{1}{(2\pi)^3} \int_\infty B_\epsilon(r_d) \exp(iK\cdot r_d) \, dr_d,$

$$k_s = 2k_0 \sin(\theta/2),$$

and the unit vectors $\hat{o}$ and $\hat{i}$ are shown in figure 2. The scattering angle θ and the polarization angle χ are shown in figure 3.

There are many possible forms for B_ϵ, but the exponential form is one which is mathematically convenient [45]

$$B_\epsilon(r_d) = \langle\epsilon_1^2\rangle \exp(-r_d/a). \tag{19}$$

This model is characterized by the variance $\langle\epsilon_1^2\rangle$ and the correlation distance a. The integral in (18) is easily evaluated to yield

$$\sigma(\theta) = \frac{k_0^4 a^3 \sin^2\chi \langle\epsilon_1^2\rangle}{2\pi(1 + 4k_0^2 a^2 \sin^2(\theta/2))^2} . \tag{20}$$

When the correlation distance a is small compared to wavelength λ, the cross section σ reduces to

$$\sigma(\theta) \approx k_0^4 a^3 \sin^2\chi \, \langle \epsilon_1^2 \rangle / (2\pi). \qquad (21)$$

The expression in (21) represents Rayleigh scattering where the scattered power is proportional to frequency to the fourth power times the correlation length to the third power.

4. ELECTRIC DIPOLE RADIATION

In the previous section we noted that the double volume integral in (16) is difficult to evaluate except when the random medium is in the far field of both the source and receiver. Dorfman [46] has treated the case where an electric dipole is located within a spherical random medium, and he was able to evaluate the intensity in the far field. In this section we elaborate on his treatment, and in section 5 we treat the analogous case for a magnetic dipole source.

4.1 Far-field Pattern

The geometry for a z-directed, electric-dipole source of moment IL is shown in figure 4. The randomness of the medium is confined to a spherical shell, $b < r < c$, where the permittivity is given by (1). The spherical shell model is idealized, but it allows us to examine near-field effects for the transmitting dipole. Following Dorfman we assume that the medium is lossless, but loss could be added to the model. Since we use the Born approximation, the coherent far field has only a θ component of electric field $E_{0\theta}$ given by [47]

$$E_{0\theta} = \frac{-i\omega\mu_0 IL \sin\theta}{4\pi r} \exp(ik_0 r). \qquad (22)$$

The coherent intensity I_c is

$$I_c = |E_{0\theta}|^2 = \frac{(\omega\mu_0 IL \sin\theta)^2}{(4\pi r)^2}. \tag{23}$$

Following Dorfman [46] we approximate B_ϵ in the form,

$$B_\epsilon(r_d) = \langle\epsilon_1^2\rangle \ell^3 \delta(r_d), \tag{24}$$

where δ is a Dirac delta function and ℓ plays the role of a correlation length. The form of B_ϵ is physically realistic only when the incident field is nearly constant over the distance ℓ. The main advantage of (24) is that it allows the integral in (16) to be evaluated analytically. If the actual correlation function is $\Gamma(r_d)$, then ℓ is obtained from

$$\ell^3 = \int_\infty \Gamma(r_d)\, dr_d. \tag{25}$$

For example, if Γ is an exponential function $\exp(-r_d/a)$, then ℓ^3 is

$$\ell^3 = \int_\infty \exp(-r_d/a)\, dr_d = 4\pi \int_0^\infty \exp(-r_d/a)\, r_d^2\, dr_d = 8\pi a^3. \tag{26}$$

If we substitute (24) into (16) and carry out the $\mathbf{r}''$ integration, we obtain

$$\langle|E_{1u}(\mathbf{r})|^2\rangle = k_0^4 \langle\epsilon_1^2\rangle \ell^3 \int_V |G_{uv}(\mathbf{r},\mathbf{r}')E_{0v}(\mathbf{r}')|^2\, d\mathbf{r}', \tag{27}$$

where V is the spherical shell volume. When the observation point is in the far field (large $k_0 r$), the Green's function in (14) or (27) simplifies considerably, and (27) simplifies to

$$\langle |E_{1\substack{\theta \\ \phi}}(r)|^2 \rangle = \frac{k_0^2 \ell^3 \langle \epsilon_1^2 \rangle}{(4\pi r)^2} \int_V |\hat{\substack{\theta \\ \phi}} \cdot E_0(r')|^2 \, dr', \tag{28}$$

where $\hat{\theta}$ and $\hat{\phi}$ are unit vectors. In the far field, $\langle |E_{1r}(r)|^2 \rangle \approx 0$.

For an electric dipole source, $E_0(r')$ is [47]

$$E_0(r') = \frac{-i\omega\mu_0 IL \exp(ik_0 r')}{4\pi r'} \{\hat{r}' \left[\frac{-2}{ik_0 r'} + \frac{2}{(ik_0 r')^2}\right] \cos\theta' + \hat{\theta}' \left[1 - \frac{1}{ik_0 r'} + \frac{1}{(ik_0 r')^2}\right] \sin\theta'\}. \tag{29}$$

If we substitute (29) into (28), we can carry out the volume integration analytically. The details are included in Appendix A, and the result is

$$\langle |E_{1\substack{\theta \\ \phi}}|^2 \rangle = k_0^3 \ell^3 \langle \epsilon_1^2 \rangle E_0^2 F_{\substack{\theta \\ \phi}}, \tag{30}$$

where $F_\theta = [k_0(c - b)(\cos^2\theta + 8 \sin^2\theta) + k_0^{-1}(b^{-1} - c^{-1})(3 \cos^2\theta + 4 \sin^2\theta) + k_0^{-3}(b^{-3} - c^{-3})(23 \cos^2\theta + 4 \sin^2\theta)]/(60 \pi)$,

$F_\phi = [k_0(c - b) + 3k_0^{-1}(b^{-1} - c^{-1}) + 15k_0^{-3}(b^{-3} - c^{-3})]/(60 \pi)$,

and $E_0 = (\omega\mu_0 IL)/(4\pi r)$. The incoherent intensity I_i is

$$I_i = \langle |E_{1\theta}|^2 \rangle + \langle |E_{1\phi}|^2 \rangle = k_0^3 \ell^3 \langle \epsilon_1^2 \rangle E_0^2 (F_\theta + F_\phi). \tag{31}$$

The ratio of the incoherent to coherent intensities is also of interest because it gives a measure of the degradation of the transmitted signal between a pair of electric dipoles:

$$I_i/I_c = k_0^3 \ell^3 \langle \epsilon_1^2 \rangle (F_\theta + F_\phi)/\sin^2\theta. \tag{32}$$

The results in (31) and (32) represent Rayleigh scattering where the incoherent intensity is proportional to third power of the correlation length, ℓ^3. This is similar to (21). However, the k_0^4 dependence is obtained only when the $k_0 c$ term is dominant in F_θ and F_ϕ. This is as expected because this is the case where far-field scattering is dominant. When near-field scattering is important, then the k_0 dependence is to some lower power. When the quasi-static term, $k_0^{-3} b^{-3}$, is dominant, the scattering is independent of k_0. If we let b approach zero, then I_i becomes infinite. This physically unrealistic result is a result of using the delta correlation function in (24). If we had chosen a finite correlation function, then I_i would have remained finite as b approached zero [46,48]. However, it is difficult to evaluate the volume integral for finite correlation functions. The results in this section are still valid as long as b is somewhat greater than ℓ.

Numerical results for the incoherent intensity are shown in figures 5 and 6. The results are normalized to CE_0^2 to make them dimensionless, and the normalization constant $C = k_0^3 \ell^3 \langle \epsilon_1^2 \rangle$. In figure 5, far-field scattering is dominant, and the maximum occurs in the broadside direction ($\theta = 90°$) as it does for the coherent component. In figure 6, near-field scattering is dominant because of the small value of $k_0 b$. Here the maximum occurs off the end of the dipole ($\theta = 0°$). An interesting feature of both cases is that the ϕ component is independent of θ. The cross-polarized ϕ component is normally zero for far-field, plane-wave scattering in the Born approximation [49], but not for the near-field case considered here.

4.2 Total Radiated Power

The total radiated power can be obtained by integrating the intensity over a sphere at infinity. The coherent power P_0 is

$$P_0 = \frac{1}{2\eta_0} \int_0^{2\pi} \int_0^{\pi} I_c \, r^2 \sin\theta \, d\theta \, d\phi. \tag{33}$$

If we substitute (23) into (33) and carry out the integrations, we obtain

$$P_0 = \eta_0 (k_0 IL)^2 / (12\pi). \tag{34}$$

The incoherent power P_1 is

$$P_1 = \frac{1}{2\eta_0} \int_0^{2\pi} \int_0^{\pi} I_i \, r^2 \sin\theta \, d\theta \, d\phi. \tag{35}$$

If we substitute (30) and (31) into (35) and carry out the integrations, we obtain

$$P_1 = \frac{\eta_0 (k_0 IL)^2 \, k_0^3 \ell^3 \langle \epsilon_1^2 \rangle}{360 \, \pi^2} [5k_0(c - b) + 5k_0^{-1}(b^{-1} - c^{-1}) + 19k_0^{-3}(b^{-3} - c^{-3})]. \tag{36}$$

The results in (31) and (36) are similar to those of Dorfman [46], but the coefficients are not the same. It is not possible to check Dorfman's derivation because he does not give any intermediate steps.

The ratio of incoherent to coherent power can be regarded roughly as a clutter-to-signal ratio and is given by

$$\frac{P_1}{P_0} = \frac{k_0^3 \ell^3 \langle \epsilon_1^2 \rangle}{30\ \pi} [5k_0(c - b) + 5k_0^{-1}(b^{-1} - c^{-1}) + 19k_0^{-3}(b^{-3} - c^{-3})]. \quad (37)$$

Because we have assumed that the observation point is in the far field of both the source and the random region, P_1/P_0 is independent of r. Normally the ratio of the incoherent to coherent intensity would increase with r if the entire medium were random [25, Ch. 6].

5. MAGNETIC DIPOLE RADIATION

In this section we extend the results of the previous section to a magnetic dipole source. A magnetic dipole source (small loop) has been suggested for the detection of long conductors in tunnels [50].

5.1 Far-field pattern

The geometry for a magnetic-dipole source is the same as that in figure 4 except that the electric-dipole source is replaced by a z-directed magnetic-dipole source of moment IA. Here we will compute the magnetic field because we anticipate reception with a magnetic dipole in borehole-to-borehole transmission. The coherent far field has only a θ component of magnetic field $H_{0\theta}$ given by [47]

$$H_{0\theta} = \frac{-k_0^2 IA \sin\theta}{4\pi r} \exp(ik_0 r). \quad (38)$$

The coherent intensity I_c is

$$I_c = |H_{0\theta}|^2 = \frac{(k_0^2 IA \sin\theta)^2}{(4\pi r)^2}. \quad (39)$$

If we again use the Born approximation and the Green's function approach [40], we can derive the magnetic field analog to (13) for the incoherent field H_1:

$$H_1(r) = \frac{-i\omega\epsilon_0}{4\pi} \int_V \epsilon_1(r') \nabla\psi \times E_0(r')\, dr', \tag{40}$$

where $\psi = \exp(ik_0|r - r'|)/|r - r'|$. As in the previous section, we approximate B_ϵ by (24) and carry out the delta function integration. In addition we make the far-field approximation and obtain the magnetic-field analog to (28):

$$\langle |H_{1\substack{\theta \\ \phi}}(r)|^2 \rangle = \frac{\omega\epsilon_0 k_0^3 \ell^3 \langle \epsilon_1^2 \rangle}{(4\pi r)^2} \int_V |\hat{\substack{\theta \\ \phi}} \cdot [\hat{r} \times E_0(r')]|^2\, dr'. \tag{41}$$

In the far field, $\langle |H_{1r}(r)|^2 \rangle \approx 0$.

For a magnetic dipole source, $E_0(r')$ is [47]

$$E_0(r') = \hat{\phi} \frac{\omega\mu_0 k_0 IA \exp(ik_0 r')}{4\pi r'} \left(1 + \frac{1}{ik_0 r'}\right) \sin\theta'. \tag{42}$$

If we substitute (42) into (41), we can carry out the volume integration analytically. The details are included in Appendix B, and the result is

$$\langle |H_{1\substack{\theta \\ \phi}}|^2 \rangle = k_0^3 \ell^3 H_0^2 G_{\substack{\theta \\ \phi}}, \tag{43}$$

where $G_\theta = [k_0(c - b) + k_0^{-1}(b^{-1} - c^{-1})]/(12\pi)$,

$$G_\phi = \cos^2\theta\, [k_0(c - b) + k_0^{-1}(b^{-1} - c^{-1})]/(12\pi),$$

and $H_0 = (\omega\epsilon_0 k_0 IA)/(4\pi r)$. The incoherent intensity I_i is

$$I_i = \langle|H_{1\theta}|^2\rangle + \langle|H_{1\phi}|^2\rangle = k_0^3 \ell^3 \langle\epsilon_1^2\rangle H_0^2 (G_\theta + G_\phi). \tag{44}$$

The ratio of the incoherent to coherent intensities is also of interest because it gives a measure of the degradation of the transmitted signal between a pair of magnetic dipoles:

$$I_i/I_c = k_0^3 \ell^3 \langle\epsilon_1^2\rangle (G_\theta + G_\phi)/\sin^2\theta. \tag{45}$$

The main difference between the magnetic and electric dipole results is that the magnetic dipole result in (43) contains no quasi-static $k_0^{-3} b^{-3}$ term. This is so because the primary electric field of the magnetic dipole in (42) contains no quasi-static r'^{-3} term. Thus the near-field scattering from random irregularities near the source is much weaker for a magnetic dipole source, and this is a potential advantage for magnetic dipole (small loop) antennas.

Numerical results for the incoherent intensity are shown in figure 7. The maximum scattering occurs off the end of the magnetic dipole ($\theta = 0°$, 90°). Again we see that there is a cross-polarized ϕ component.

5.2 Total Radiated Power

The total radiated power can be obtained by integrating the intensity over a sphere at infinity. The coherent power P_0 is

$$P_0 = \frac{\eta_0}{2} \int_0^{2\pi} \int_0^{\pi} I_c \, r^2 \sin\theta \, d\theta \, d\phi. \tag{46}$$

If we substitute (39) into (46) and carry out the integrations, we obtain

$$P_0 = \eta_0 (k_0^2 IA)^2/(12\pi). \tag{47}$$

The incoherent power P_1 is

$$P_1 = \frac{\eta_0}{2} \int_0^{2\pi} \int_0^{\pi} I_i \, r^2 \sin\theta \, d\theta \, d\phi. \tag{48}$$

If we substitute (43) and (44) into (48) and carry out the integrations, we obtain

$$P_1 = \frac{\eta_0 (k_0^2 IA)^2 \, k_0^3 \ell^3 \langle \epsilon_1^2 \rangle}{72 \, \pi^2} [k_0(c - b) + k_0^{-1}(b^{-1} - c^{-1})]. \tag{49}$$

The ratio of incoherent to coherent power can be regarded as a clutter-to-signal ratio and is given by

$$\frac{P_1}{P_0} = \frac{k_0^2 \ell^3 \langle \epsilon_1^2 \rangle}{6\pi} [k_0(c - b) + k_0^{-1}(b^{-1} - c^{-1})]. \tag{50}$$

The power ratio in (50) agrees with the first two terms of the electric dipole result in (37). The difference is that the electric dipole result in (37) contains an additional quasi-static term proportional to $k_0^{-3}(b^{-3} - c^{-3})$. Since the magnetic dipole result in (48) does not contain this term, a magnetic dipole does not scatter as much power when near-field scattering is dominant (small $k_0 b$). Numerical results for the power ratios are shown in figure 8 for both a vertical magnetic dipole (VMD) and a vertical electric dipole (VED). For large $k_0 b$, the results are the same for the two dipole types. For small $k_0 b$, the incoherent power rises rapidly for the VED because of the additional quasi-static term in (37).

If we write the two power ratios for the small $k_0 b$ limit, we obtain

$$\frac{P_1}{P_0} \approx \frac{k_0^2 \ell^3}{b} \cdot \frac{\langle \epsilon_1^2 \rangle}{6\pi}, \qquad \text{(VMD)},$$

$$\frac{P_1}{P_0} \approx \frac{\ell^3}{b^3} \cdot \frac{19 \langle \epsilon_1^2 \rangle}{30\ \pi}, \qquad \text{(VED)}. \tag{51}$$

It is clear from (51) that the incoherent power increases much faster (b^{-3} dependence) for decreasing b for the VED than for the VMD. Also, the power ratio is independent of frequency for the VED, but is proportional to frequency squared for the VMD. Both of these comparisons indicate a possible advantage for the VMD when the source is located within an inhomogeneous region. (By reciprocity the same conclusions apply when the receiving antenna is located within an inhomogeneous region.) It is interesting that similar conclusions hold for near-field conduction losses. Input impedance calculations for a VMD within a spherical [51] or cylindrical [52] cavity in a conducting medium show the same b^{-1} dependence as (51). Input impedance calculations for a VED close to a conducting half space [53] show the same b^{-3} dependence as (49). The frequency dependences for dipoles in a lossy medium are somewhat different from those in (51), but even there the VED shows more loss at low frequencies [52].

6. TRANSMISSION BETWEEN VERTICAL DIPOLES

If the transmitting and receiving antennas are located in an infinite random medium, then the integrals arising from the Born approximation are difficult to evaluate and might not even converge. However, by neglecting backscatter and by making far-field approximations, Ishimaru [25, Ch. 6] has developed some useful approximations. In this section we specialize his results to two vertical dipoles in a random continuum. In section 6.1 we consider cw transmission, and in section 6.2 we consider pulse transmission.

6.1 CW Transmission

The geometry for transmission between vertical dipoles is shown in figure 9. Ishimaru writes the ratio of the received coherent power P_c to the transmitted power P_t as

$$\frac{P_c}{P_t} = \frac{\lambda^2}{(4\pi)^2} \frac{G_t G_r}{L^2} e^{-\gamma}, \tag{52}$$

where G_t and G_r are the gains of the transmitting and receiving antennas, and $e^{-\gamma}$ represents attenuation of the medium due to scattering. For a lossy medium, $e^{-\gamma}$ would also include absorption loss. For the geometry in figure 9, we have $L = d/\cos\alpha$ and $G_t = G_r = (3/2)\cos\alpha$. The results in this section apply to both electric and magnetic dipoles because both have the same far-field pattern, and we can rewrite (52) as

$$\frac{P_c}{P_t} = \frac{\lambda^2}{(4\pi)^2} \frac{(3/2)^2 \cos^4\alpha}{d^2} e^{-\gamma}. \tag{53}$$

An approximate ratio of the incoherent power P_i to the coherent power P_c is given by Ishimaru:

$$P_i/P_c = \gamma = \rho\sigma_s L, \tag{54}$$

where the total scattering cross section per unit volume $\rho\sigma_s$ is given by the integral of the bistatic cross section over 4π steradians [25]

$$\rho\sigma_s = \int_{4\pi} \sigma(\hat{o},\hat{i})\, d\Omega, \tag{55}$$

and σ is given by (18). For the exponential model of B_ϵ given in (19), σ is given by (20). In general the integration in (55) is difficult to carry

out, but approximate results for the limits of small $k_0 a$ and large $k_0 a$ are given in Appendix C. If these results are substituted into (54), the following results are obtained for the ratio of the incoherent to coherent power:

$$\frac{P_i}{P_c} \approx \begin{cases} (4/3)\langle \epsilon_1^2 \rangle (k_0 a)^3 k_0 L, & k_0 a \ll 1 \\ (1/2)\langle \epsilon_1^2 \rangle (k_0 a) k_0 L, & k_0 a \gg 1. \end{cases} \tag{56}$$

The approximate results in (56) also agree with Ishimaru's plane-wave results, and for this weak scattering case the power ratio is proportional to the path length. As usual the power ratio is also proportional to the variance $\langle \epsilon_1^2 \rangle$.

6.2 Pulse Transmission

Pulse transmission is also of interest in tunnel detection, and arrival time and pulse dispersion are useful quantities in tomographic imaging [7]. Ishimaru [25, Sec. 6.5] has obtained an approximate result for pulse propagation between a pair of antennas, and we apply his result to the geometry in figure 9.

The transmitted pulse has energy E_0 and varies with time as the delta function $\delta(t)$. The received coherent intensity $I_c(t)$ has the same time variation with a time delay:

$$I_c(t) = P_c \, E_0 \, \delta(t - \frac{L}{c_0}), \tag{57}$$

where c_0 is the velocity in the background homogeneous medium and P_c is given by (53).

The received incoherent intensity $I_i(t)$ is obtained approximately by a saddle point evaluation [25, Sec. 6.5]:

$$I_i(t) = 2(\pi)^{1/2} P_c E_0 \alpha_p \rho\sigma_s c_0 \exp[-(c_0/L)(8\alpha_p - \rho\sigma_s L)(t - L/c_0)]. \quad (58)$$

The result in (58) applies for $t > L/c_0$, and $I_i(t) = 0$ for $t < L/c_0$. For large particle size D, α_p and the exponential time constant τ are given by

$$\alpha_p \approx (\frac{\pi D}{2\lambda})^2 \text{ and } \tau \approx L/(8c_0\alpha_p) \approx L\lambda^2/(2\pi^2 c_0 D^2). \quad (59)$$

The total incoherent energy E_i in the received pulse is given by

$$E_i = \int_0^\infty I_i(t)\, dt \approx P_c E_0 \rho\sigma_s L\, (\pi^{1/2}/4). \quad (60)$$

The ratio of the incoherent to coherent energy in the received pulse is

$$E_i/E_c \approx (\pi^{1/2}/4)\, \rho\sigma_s L. \quad (61)$$

This result is the same as the cw result in (54) except for a constant factor $(\pi^{1/2}/4)$.

For small particle sizes ($D \ll \lambda$), α_p and the exponential time constant are given by

$$\alpha_p \approx \frac{2.77}{(\pi/2)^2} \approx 1.12 \text{ and } \tau \approx L/(8c_0\alpha_p) \approx L/(9c_0). \quad (62)$$

In obtaining (62) from Ishimaru's result, we have made the assumption that the beamwidth for small particle scattering is $\pi/2$. This result for the decay time constant is quite different from the result in (59), but in both cases the length of the incoherent pulse is proportional to the path length L. Thus for either large or small particles, the relative size of the incoherent pulse grows in both amplitude and length as the path length L

increases. This is in agreement with the cw description of the incoherent wave in Ishimaru [25, Ch. 6].

7. CONCLUSIONS AND RECOMMENDATIONS

This report represents a first effort at modelling clutter in subsurface electromagnetic applications, particularly for tunnel detection. While deterministic earth models [22] can be used for modelling clutter, it appears that random media models [25] are more versatile and require less information about the inhomogeneous earth. The Born approximation is the simplest approach to computing the incoherent field that is generated in a random medium, but even with the Born approximation the calculations are difficult for real antenna applications where the fields are not plane waves. The main difficulty arises in evaluating the volume integrals of the type discussed in Section 3.2.

However, useful results can be obtained when only the transmitting antenna is located close to the random medium, and specific results for electric and magnetic dipoles are derived in Sections 4 and 5. The pattern of the incoherent intensity radiated by either type of dipole is different from that of the coherent intensity. A practical result is that electric dipoles are more strongly affected by near-field inhomogeneities than are magnetic dipoles. Similar results have been previously obtained for the effects of near-field conduction losses for electric and magnetic dipole sources [52].

There are many unsolved problems in clutter analysis. The isotropic correlation functions that we have used are not applicable to flat or fracture irregularities, and fractures are thought to be the most important scatterers in tunnel detection applications [54]. It remains to be seen whether an anisotropic correlation function or a totally new approach is required to model fractures. Even when clutter is adequately modelled, the question of how to image or detect tunnels in the presence of clutter remains. The general problem of imaging in a random medium has been studied [55], but the specific application of tunnel detection might require special techniques to enhance the tunnel signal and to reduce the clutter effects.

It seems likely that a combination of further analysis coupled with EM measurements at a well characterized site will yield the most rapid progress on the overall tunnel detection problem.

8. ACKNOWLEDGMENT

This research was supported by the U.S. Army Belvoir RD&E Center.

9. REFERENCES

[1] Keller, G.V.; Frischnecht, F.C. Electrical Methods in Geophysical Prospecting. New York: Pergamon Press; 1966.

[2] Kaufman, A.A.; Keller, G.V. The Magnetotelluric Sounding Method. Amsterdam: Elsevier Scientific Pub. Co.; 1981.

[3] Kaufman, A.A.; Keller, G.V. Frequency and Transient Soundings. Amsterdam: Elsevier Scientific Pub. Co.; 1983.

[4] Murphy, J.N.; Parkinson, H.E. Underground mine communications. Proc. IEEE, 66: 26-50; 1978.

[5] Delogne, P. Leaky Feeder and Subsurface Radio Communications. Stevenage: Peter Peregrinus Ltd.; 1982.

[6] Lytle, R.J.; Laine, E.F.; Lager, D.L.; Davis, D.T. Cross-borehole electromagnetic probing to locate high-contrast anomalies. Geophys., 44: 1667-1676; 1979.

[7] Olhoeft, G.R. Interpretation of hole-to-hole radar measurements. Third Technical Symposium on Tunnel Detection. Golden, CO: Jan. 12-15, 1988.

[8] Stolarczyk, L.G. Long feature tunnel detection methodologies using phase coherent electromagnetic instrumentation. Third Technical Symposium on Tunnel Detection. Golden, CO: Jan. 12-15, 1988.

[9] Chan, L.C.; Moffatt, D.L.; Peters, L. A characterization of subsurface radar targets. Proc. IEEE, 67: 991-1000; 1979.

[10] Hill, D.A. Electromagnetic scattering by buried objects of low contrast. IEEE Trans. Geosci. Rem. Sens., GE-26: 195-203; 1988.

[11] Brekhovskikh, L. Waves in Layered Media. New York: Academic Press; 1960.

[12] Wait, J.R. Electromagnetic Waves in Stratified Media. New York: Pergamon Press; 1962.

[13] Wait, J.R.; Hill, D.A. Fields of a horizontal loop of arbitrary shape buried in a two-layer earth. Rad. Sci., 15: 903-912; 1980.

[14] Hill, D.A. Radio propagation in a coal seam and the inverse problem. J. Res. NBS, 89: 385-394; 1984.

[15] Fry, R.; Schotsch, J.; Stolarczyk, L.G. The radio imaging method (RIM) - a means of detecting and imaging anomalous geologic structures in a coal seam. 4th Conference on ground control in mining. Morgantown, WV: July 22-24, 1985.

[16] Hill, D.A. Effect of a thin conducting sheet on the fields of a buried magnetic dipole. Electromagnetics, 7: 71-79; 1987.

[17] Schaber, G.G.; McCauley, J.F.; Breed, C.S.; Olhoeft, G.R. Shuttle imaging radar: physical controls on signal penetration and subsurface scattering in the eastern Sahara. IEEE Trans. Geosci. Rem. Sens., GE-24: 603-623; 1986.

[18] Lager, D.L.; Lytle, R.J. Determining a subsurface electromagnetic profile from high-frequency measurements by applying reconstruction-technique algorithms. Rad. Sci., 12: 249-260; 1977.

[19] Radcliff, R.D.; Balanis, C.A. Reconstruction algorithms for geophysical applications in noisy environments. Proc. IEEE, 67: 1060-1064; 1979.

[20] Lee, T.K.; Kim, S.Y.; Ra, J.W. Resonant scattering of CW electromagnetic wave by an underground tunnel of circular cross section. Third Technical Symposium on Tunnel Detection. Golden, CO: Jan. 12-15, 1988.

[21] Shope, S.; Greenfield, R. Electromagnetic cross-hole tomography for tunnel detection. Third Technical Symposium on Tunnel Detection. Golden, CO: Jan. 12-15, 1988.

[22] Eaton, P.A.; Hohmann, G.W. An evaluation of electromagnetic methods in the presence of geologic noise. Geophys., 52; 1106-1126, 1987.

[23] Hill, D.A.; Wait, J.R. The electromagnetic response of a buried sphere for buried-dipole excitation. Rad. Sci., 8: 813-818, 1973.

[24] Hill, D.A.; Wait, J.R. Perturbation of magnetic dipole fields by a perfectly conducting prolate spheroid. Rad. Sci., 9; 71-73, 1974.

[25] Ishimaru, A. Wave Propagation and Scattering in Random Media. New York: Academic Press; 1978.

[26] Battan, L.J. Radar Obsvervation of the Atmosphere. Chicago: Univ. of Chicago Press; 1973.

[27] Tatarskii, V.I. The Effects of the Turbulent Atmosphere on Wave Propagation. Jerusalem: Israel Program for Scientific Translations; 1971.

[28] Davenport, Jr., W.B.; Root, W.L. Random Signals and Noise. New York: McGraw-Hill; 1958.

[29] Besieris, I.M. On the applicability of continuous scattering methods to discrete scattering problems. AGARD Conference Proceedings No. 419, Scattering and Propagation in Random Media. Rome, Italy: May 18-22, 1988.

[30] Fung, A.K.; Fung, H.S. Application of first-order reformalization method to scattering from a vegetation-like half-space. IEEE Trans. Geosci. Electron., GE-15: 189-195; 1977.

[31] Tsang, L.; Kong, J.A. Wave theory for microwave remote sensing of a half-space random medium with three-dimensional variations. Rad. Sci., 14: 359-369; 1979.

[32] Karal, Jr., F.C.; Keller, J.B. Elastic, electromagnetic, and other waves in a random medium. J. Math. Phys., 5: 537-547; 1964.

[33] Keller, J.B.; Karal, Jr., F.C. Effective dielectric constant, permeablility, and conductivity of a random medium and the velocity and attenuation coefficient of coherent waves. J. Math. Phys., 7: 661-670; 1966.

[34] Roth, L.E.; Elachi, C. Coherent electromagnetic losses by scattering from volume irregularities. IEEE Trans. Ant. Propagat., AP-23: 674-675; 1975.

[35] Frisch, V. Wave propagation in random media. Probabilistic Methods in Applied Mathematics, Vol. 1 (A.T. Barucha-Reid, ed.). New York: Academic Press; 1968.

[36] Rosenbaun, S. The mean Green's function: a non-linear approximation. Rad. Sci., 6: 379-386; 1971.

[37] Dence, D.; Spence, J.E. Wave propagation in random anisotropic media. Probabilistic Methods in Applied Mathematics, Vol. 3 (A.T. Barucha-Reid, ed.). New York: Academic Press; 1973.

[38] Tsang, L.; Kong, J.A. Microwave remote sensing of a two-layer random medium. IEEE Trans. Ant. Propagat., AP-24: 283-288; 1976.

[39] Lee, J.K.; Mudaliar, S. Backscattering coefficients of a half-space anisotropic random medium by the multiple-scattering theory. Rad. Sci., 23: 429-422; 1988.

[40] Tai, C.T. Dyadic Green's Functions in Electromagnetic Theory. Scranton, PA: Intext Ed. Pub.; 1971.

[41] Van Bladel, J. Some remarks on Green's dyadic for infinite space. IRE Trans. Ant. Propagat., AP-9: 563-566; 1961.

[42] Yaghjian, A.D. Electric dyadic Green's functions in the source region. Proc. IEEE, 68: 248-263; 1980.

[43] Varvatsis, A.D.; Sancer, M.I. On the renormalization method in random wave propagation. Rad. Sci., 6: 87-97; 1971.

[44] Stogryn, A. Electromagnetic scattering by random dielectric constant fluctuations in a bounded medium. Rad. Sci., 9: 509-518; 1974.

[45] Booker, H.G.; Gordon, W.E. A theory of radio scattering in the troposphere. Proc. IRE, 38: 401-412; 1950.

[46] Dorfman, Y.M. Electric dipole radiation in a randomly nonuniform medium. Rad. Engr. Electron. Phys., 15: 1105-1106; 1970.

[47] Harrington, R.F. Time-Harmonic Electromagnetic Fields. New York: McGraw-Hill; 1961.

[48] Dokuchaev, V.P.; Ryzhov, Y.A.; Tamoikin, V.V. Radiation of an elementary dipole in a randomly inhomogeneous medium. Radiophysics and Quantum Electronics, 12: 1182-1188; 1969.

[49] Ulaby, F.T.; Moore, R.K.; Fung, A.K. Microwave Remote Sensing, Vol. III. Norwood, MA: Artech House; 1986. Sec. 13-3.

[50] Hill, D.A. Magnetic dipole excitation of a long conductor in a lossy medium. IEEE Trans. Geosci. Rem. Sens., 26: to be published; 1988.

[51] Wait, J.R.; Spies, K.P. A note on the insulated loop antenna immersed in a conducting medium. Rad. Sci. J. Res. NBS, 68D: 1249-1250; 1964.

[52] Hill, D.A.; Wait, J.R. The impedance of dipoles in a circular tunnel with an axial conductor. IEEE Trans. Geosci. Electron., GE-16: 118-126; 1978.

[53] Wait, J.R. Impedance characteristics of electric dipoles over a conducting half-space. Rad. Sci., 4: 971-975; 1969.

[54] Olhoeft, G.R. U.S. Geological Survey, Denver, CO 80225-0046. Private communication, 1988.

[55] Ishimaru, A. Imaging in random media. Proc. URSI International Symposium on Electromagnetic Theory: 59-62. Budapest, Hungary; 1986.

APPENDIX A - VOLUME INTEGRATION FOR ELECTRIC DIPOLE SOURCE

The unit vectors in (28) can be written in terms of the Cartesian unit vectors:

$$\hat{\theta} = \hat{\mathbf{x}}\cos\phi\cos\theta + \hat{\mathbf{y}}\sin\phi\cos\theta - \hat{\mathbf{z}}\sin\theta,$$

$$\hat{\phi} = -\hat{\mathbf{x}}\sin\phi + \hat{\mathbf{y}}\cos\phi. \tag{A1}$$

We can write the primed unit vectors in (29) in a similar manner:

$$\hat{\theta}' = \hat{\mathbf{x}}\cos\phi'\cos\theta' + \hat{\mathbf{y}}\sin\phi'\cos\theta' - \hat{\mathbf{z}}\sin\theta',$$

$$\hat{\mathbf{r}}' = \hat{\mathbf{x}}\cos\phi'\sin\theta' + \hat{\mathbf{y}}\sin\phi'\sin\theta' + \hat{\mathbf{z}}\cos\theta'. \tag{A2}$$

Using (A1) and (A2), we can evaluate the dot products required in (28):

$$\hat{\theta}\cdot\hat{\theta}' = \cos(\phi-\phi')\cos\theta\cos\theta' + \sin\theta\sin\theta',$$

$$\hat{\theta}\cdot\hat{\mathbf{r}}' = \cos(\phi-\phi')\cos\theta\sin\theta' - \sin\theta\sin\theta',$$

$$\hat{\phi}\cdot\hat{\theta}' = \sin(\phi'-\phi)\cos\theta', \tag{A3}$$

$$\hat{\phi}\cdot\hat{\mathbf{r}}' = \sin(\phi'-\phi).$$

The volume integral in (28) can be written

$$\int_V \left|\begin{matrix}\hat{\theta}\\ \hat{\phi}\end{matrix}\cdot \mathbf{E}_0(\mathbf{r}')\right|^2 d\mathbf{r}' = \int_b^c \int_0^{2\pi} \int_0^{\pi} \left|\begin{matrix}\hat{\theta}\\ \hat{\phi}\end{matrix}\cdot \mathbf{E}_0(\mathbf{r}')\right|^2 r'^2 \sin\theta'\, d\theta' d\phi' dr'. \tag{A4}$$

The r' integration involves only powers of r' and can be done analytically. The ϕ' and θ' integrations involve only trigonometric functions, and they

can also be done analytically. When we substitute (A1)-(A3) and (29) into (A4) and carry out the r′, ϕ', and θ' integrations, we obtain the final result in (30).

APPENDIX B - VOLUME INTEGRATION FOR MAGNETIC DIPOLE SOURCE

The dot products involving the unit vectors in (41) can be written

$$\hat{\theta}\cdot(\hat{\mathbf{r}}\times\hat{\phi}') = \hat{\phi}'\cdot(\hat{\theta}\times\hat{\mathbf{r}}) = -\hat{\phi}'\cdot\hat{\phi},$$

$$\hat{\phi}\cdot(\hat{\mathbf{r}}\times\hat{\phi}') = \hat{\phi}'\cdot(\hat{\phi}\times\hat{\mathbf{r}}) = \hat{\phi}'\cdot\hat{\theta}. \tag{B1}$$

The dot products in (B1) are evaluated in the same manner as in Appendix A, and the results are

$$-\hat{\phi}'\cdot\hat{\phi} = -\cos(\phi-\phi'),$$

$$\hat{\phi}'\cdot\hat{\theta} = \sin(\phi-\phi')\cos\theta. \tag{B2}$$

The volume integral in (41) takes the same general form as that in (A4), and again the r′, ϕ', and θ' integrations can be done analytically. When we substitute (B1), (B2), and (42) into (41) and carry out the integrations, we obtain the final result in (41).

APPENDIX C - ANGULAR INTEGRATION FOR SCATTERING CROSS SECTION

The first step in the evaluation of (55) is to write the solid angle integration in spherical coordinates:

$$\rho\sigma_s = \int_0^{2\pi}\int_0^{\pi} \sigma \sin\theta \, d\theta \, d\phi, \tag{C1}$$

where σ is given by (20) and the geometry is shown in figure 3. The $\sin^2\chi$ factor can be written in terms of ϕ and θ:

$$\sin^2\chi = 1 - \cos^2\phi \sin^2\theta. \tag{C2}$$

For small values of k_0a, we can approximate (C1) in the following form:

$$\rho\sigma_s \approx \frac{k_0^4 a^3 \langle\epsilon_1^2\rangle}{2\pi} \int_0^{2\pi}\int_0^{\pi} (1 - \cos^2\phi \sin^2\theta) \sin\theta \, d\theta \, d\phi. \tag{C3}$$

The θ and ϕ integrations in (C3) can be done in closed form to yield the desired final result for small k_0a:

$$\rho\sigma_s \approx (4/3) k_0^4 a^3 \langle\epsilon_1^2\rangle. \tag{C4}$$

When k_0a is large, we make small-angle approximations for $\sin^2\theta$ and $\sin^2(\theta/2)$, and (C1) can be approximated

$$\rho\sigma_s \approx \frac{k_0^4 a^3 \langle\epsilon_1^2\rangle}{2\pi} \int_0^{2\pi}\int_0^{\Delta} \frac{\theta \, d\theta \, d\phi}{(1 + k_0^2 a^2 \theta^2)^2}, \tag{C5}$$

where Δ is chosen large enough to include the significant portion of the integrand, but small enough for the small θ approximations to be valid. The ϕ integration in (C5) contributes a 2π factor. The θ integration is evaluated by substitution:

$$\int_0^{\Delta} \frac{\theta \, d\theta}{(1 + k_0^2 a^2 \theta^2)^2} = \int_0^{\Delta^2} \frac{dx}{2(1 + k_0^2 a^2 x)^2} = \frac{1}{2k_0^2 a^2} \left(1 - \frac{1}{1 + k_0^2 a^2 \Delta^2}\right). \tag{C6}$$

We can neglect the second term in the parentheses, and the desired final result for large $k_0 a$ is

$$\rho\sigma_s \approx k_0^2 a \langle \epsilon_1^2 \rangle / 2. \tag{C7}$$

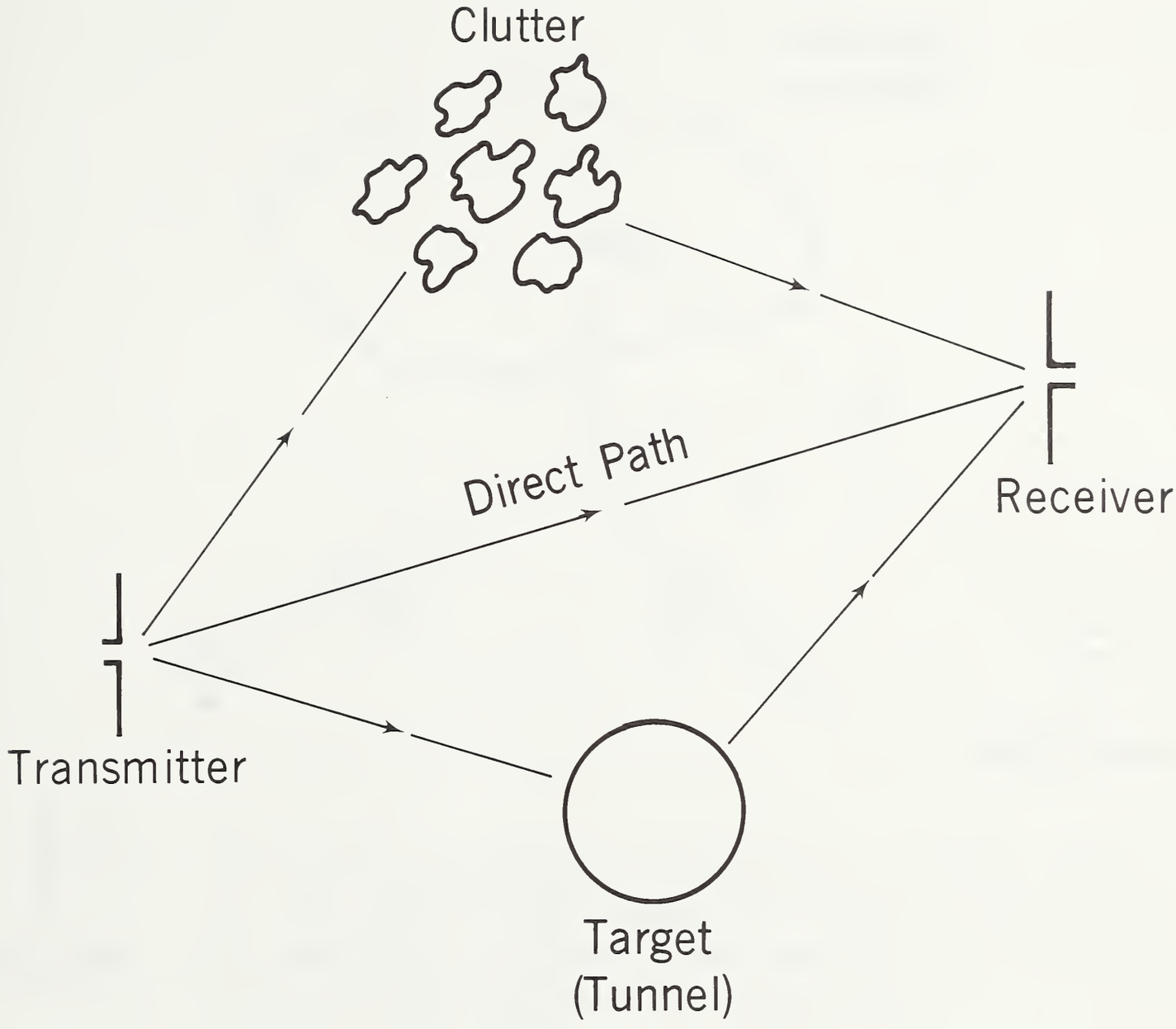

Figure 1. Typical geometry for tunnel detection in the presence of clutter.

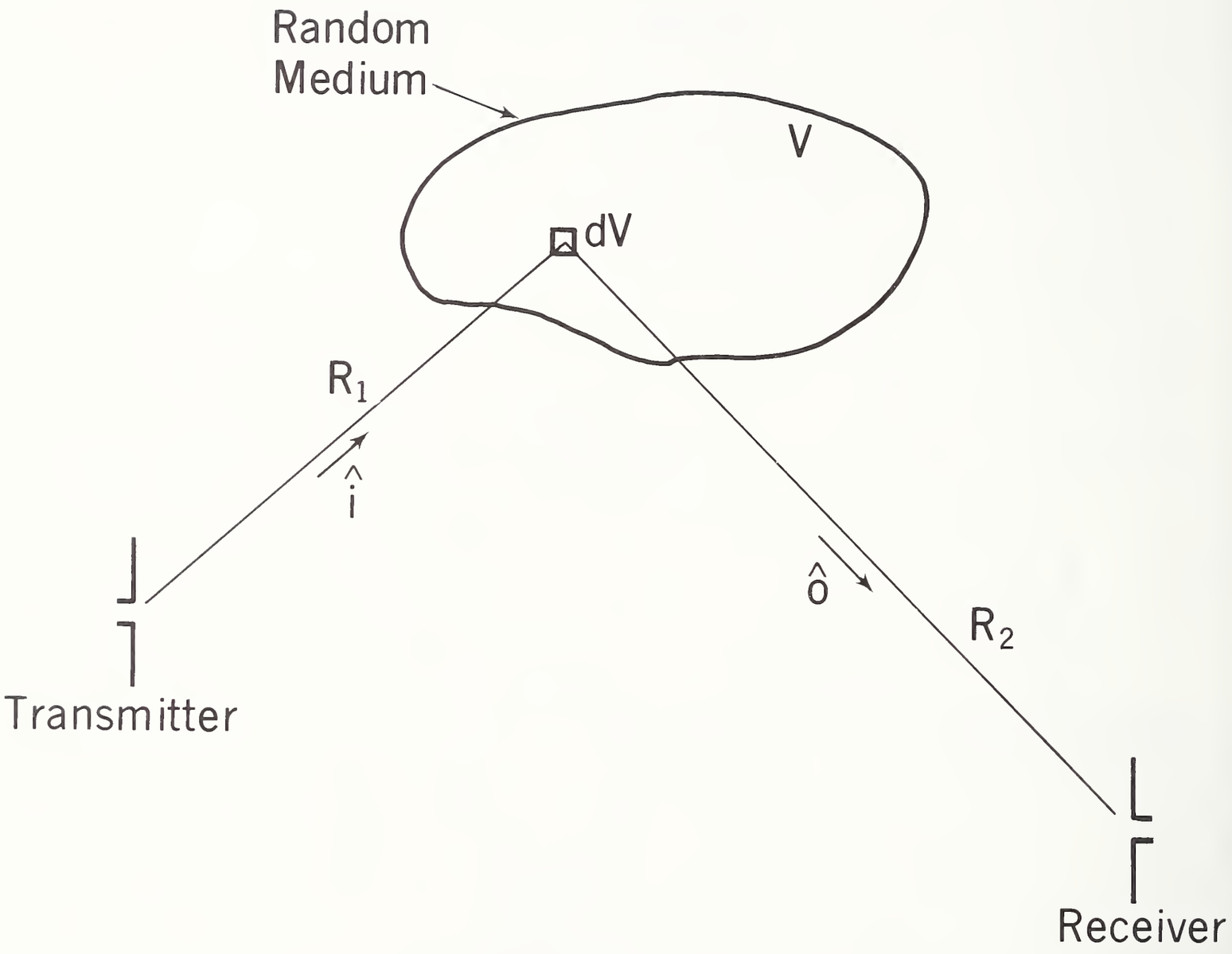

Figure 2. Geometry for scattering by an elemental volume dV in a random medium.

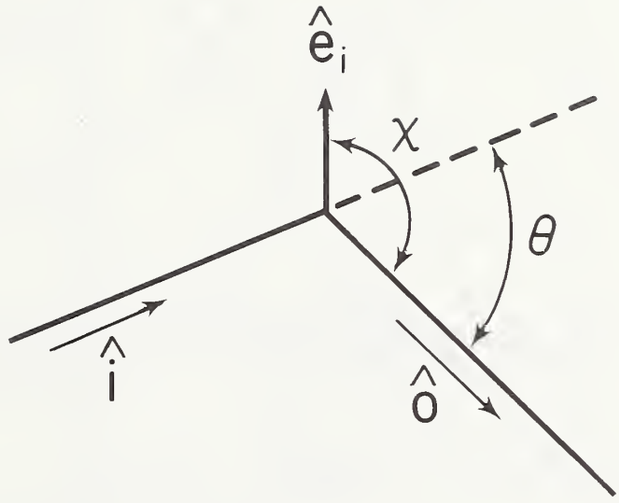

Figure 3. Geometry for the scattering angle θ and the polarization angle χ. The unit vectors $\hat{i}$ and $\hat{o}$ indicate the propagation directions of the incident and scattered waves, and the unit vector $\hat{e}_i$ indicates the polarization of the incident wave.

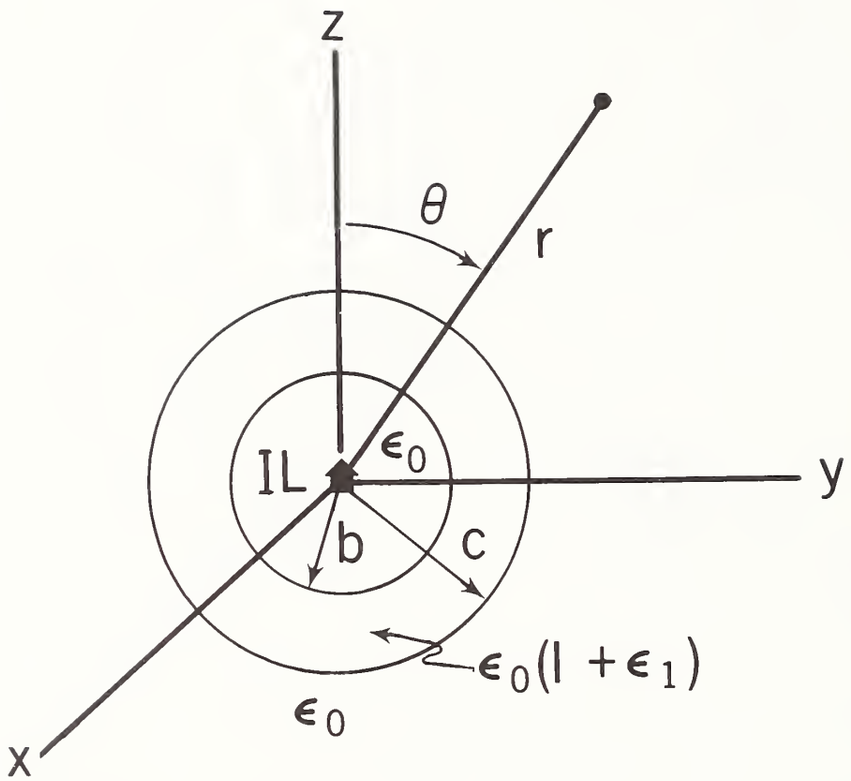

Figure 4. An electric dipole source at the center of a random medium with spherical boundaries.

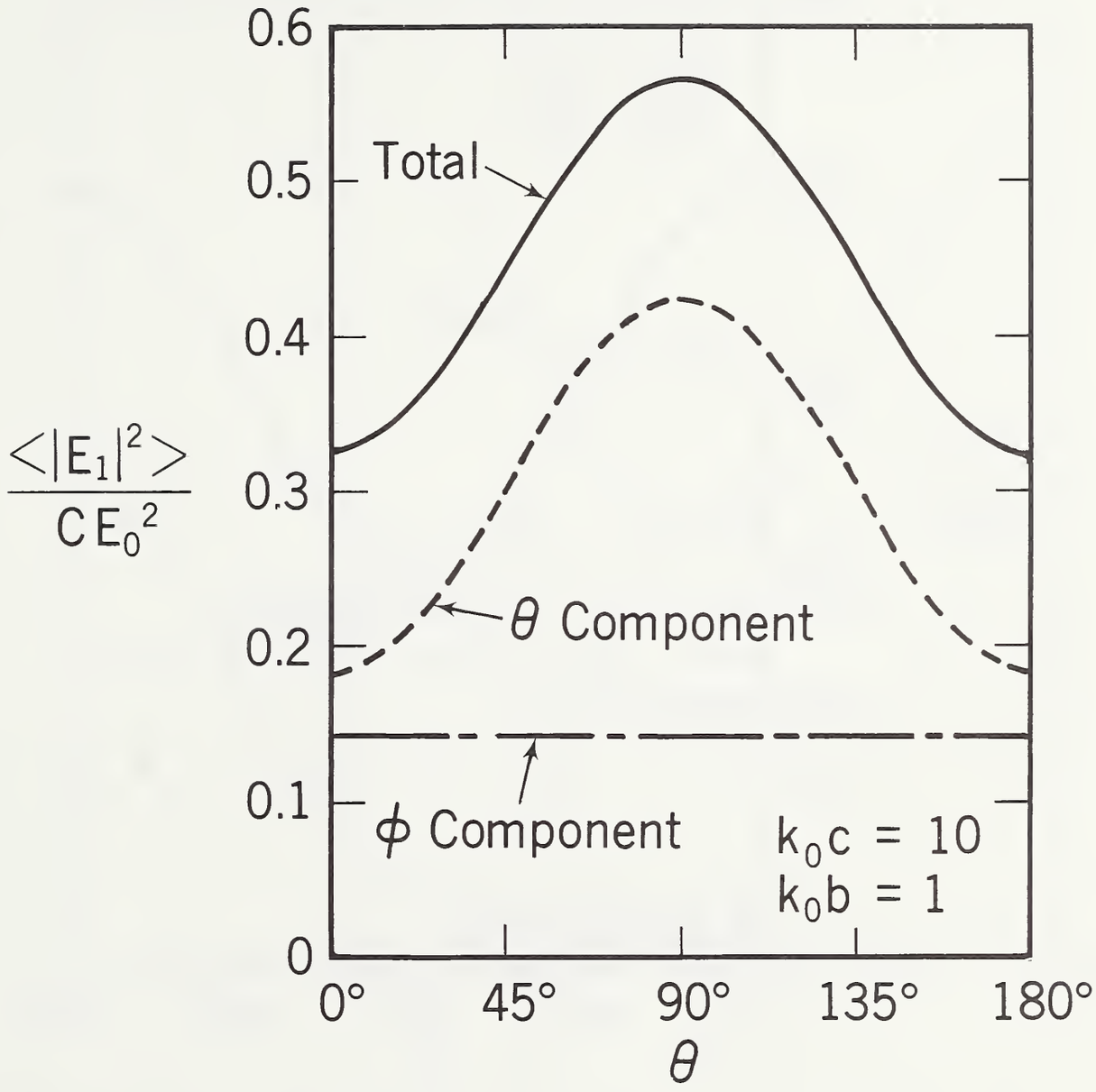

Figure 5. Radiation pattern of the incoherent scattered field for an electric dipole source.

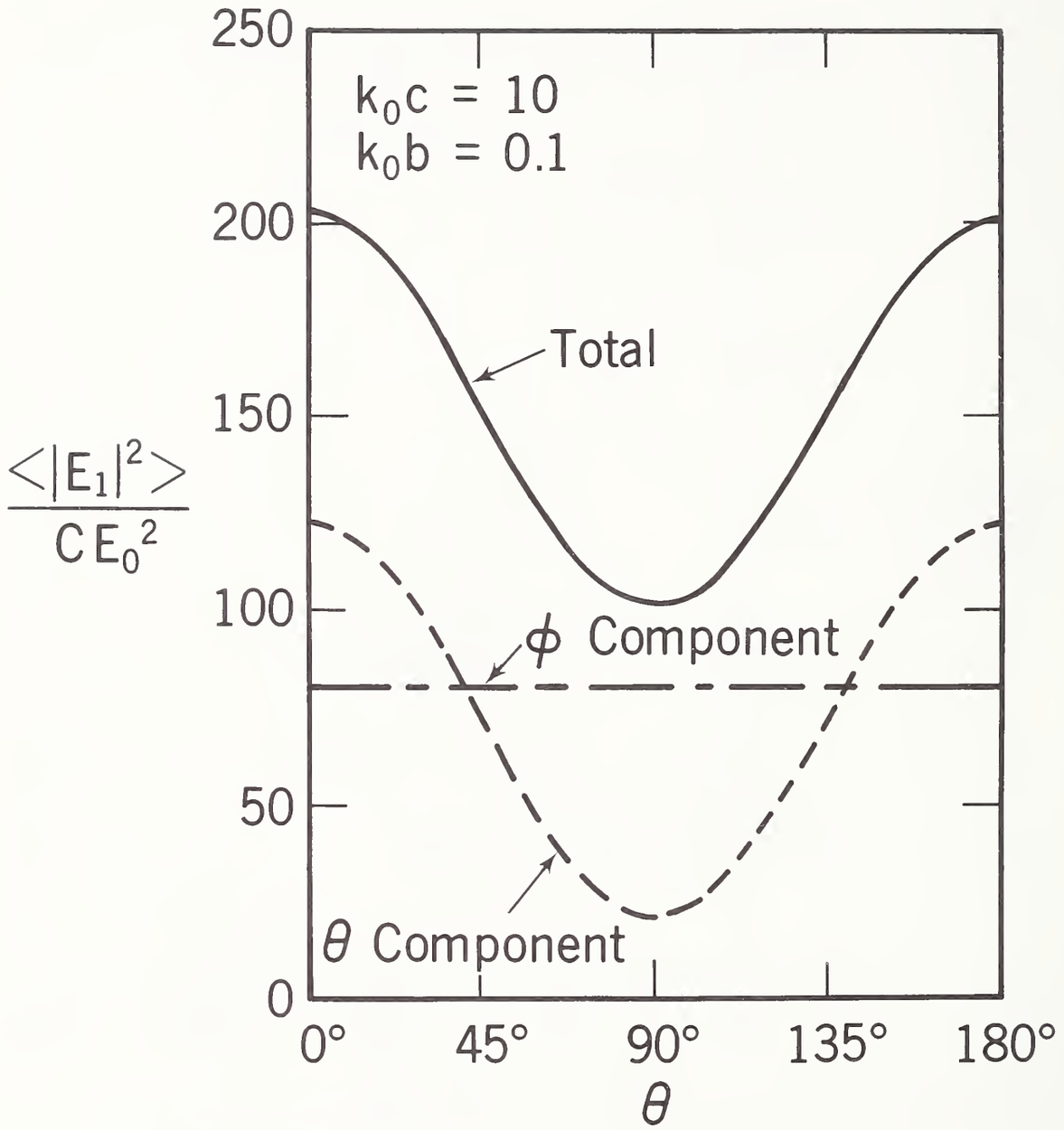

Figure 6. Radiation pattern of the incoherent field of an electric dipole for a smaller value of k_0b.

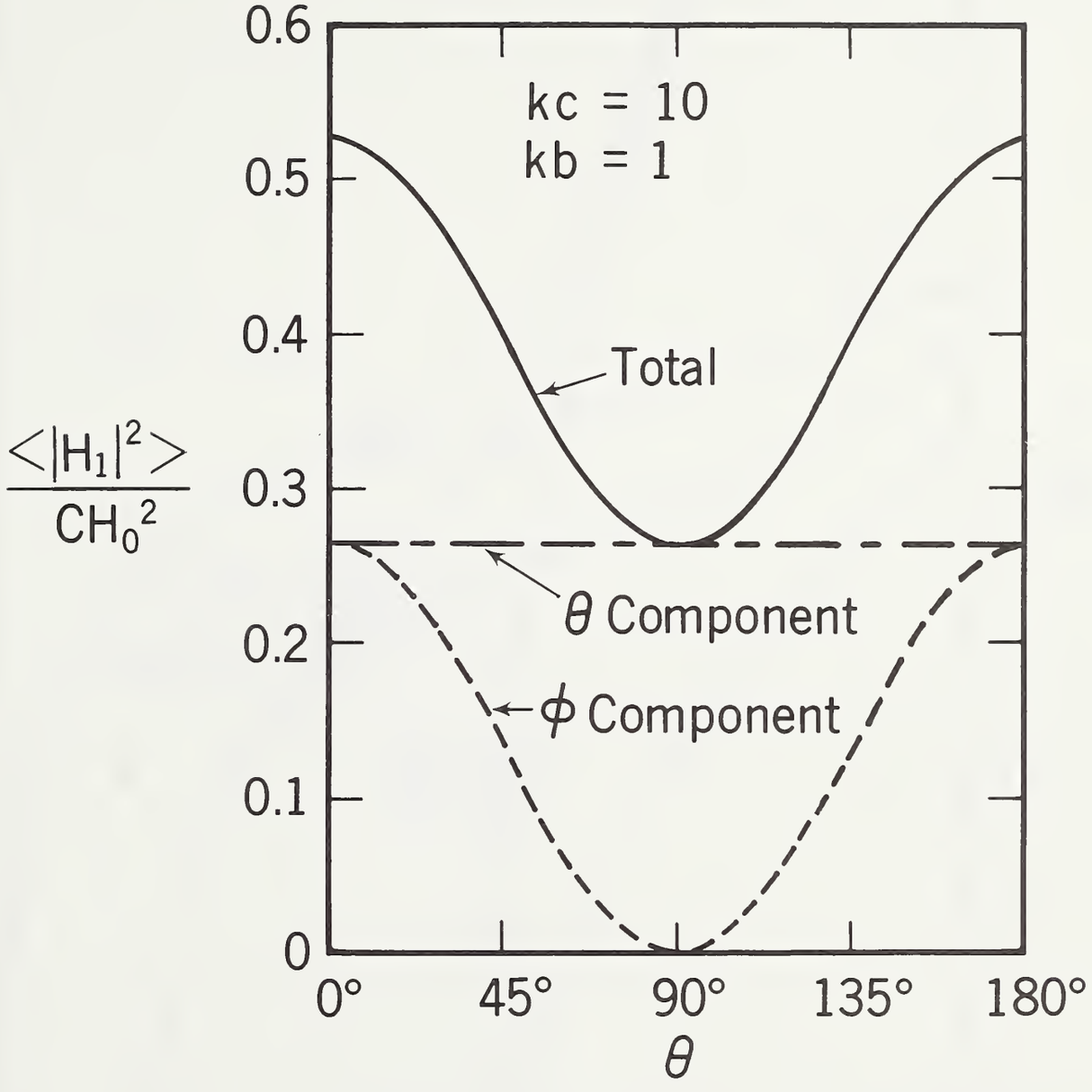

Figure 7. Radiation pattern of the incoherent field of a magnetic dipole source.

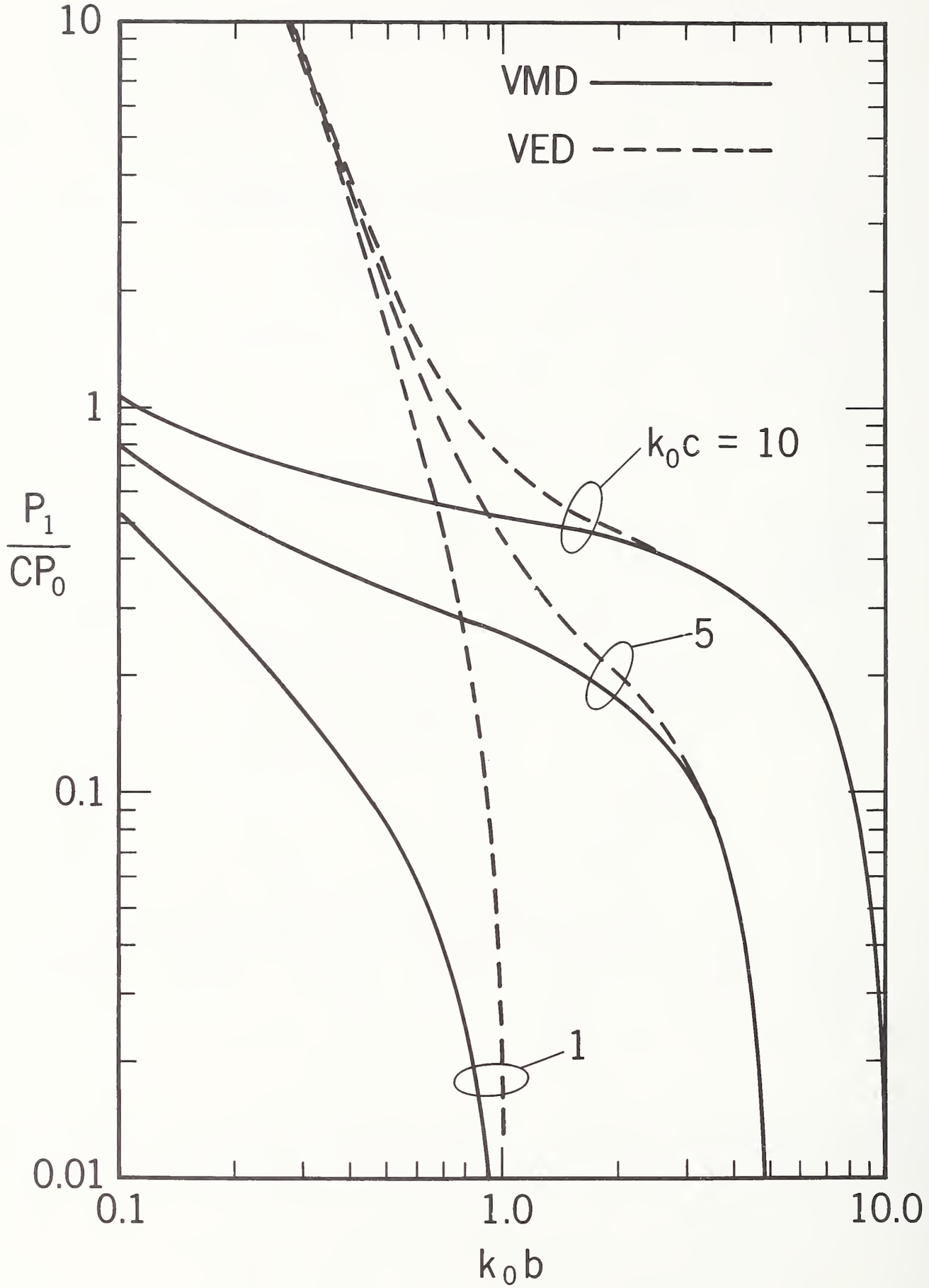

Figure 8. Ratio of radiated incoherent to coherent power for electric and magnetic dipole sources.

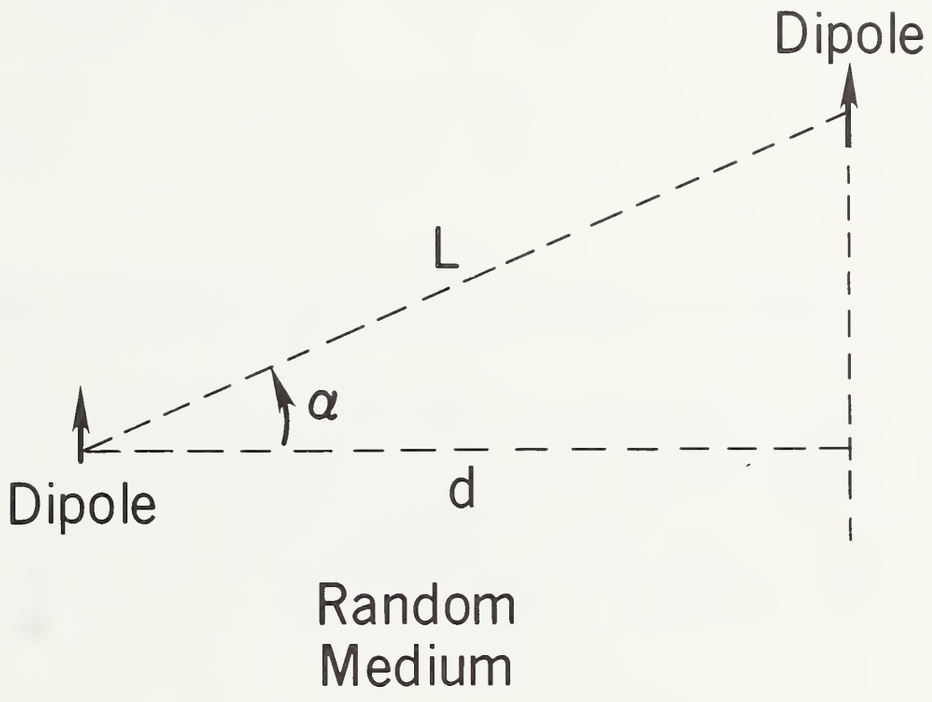

Figure 9. Geometry for dipole-to-dipole transmission in a random medium.

NBS-114A (REV. 2-8C)

U.S. DEPT. OF COMM. BIBLIOGRAPHIC DATA SHEET (See instructions)	1. PUBLICATION OR REPORT NO. NISTIR 89-3909	2. Performing Organ. Report No.	3. Publication Date February 1989

4. TITLE AND SUBTITLE

Clutter Models for Subsurface Electromagnetic Applications

5. AUTHOR(S)

David A. Hill

6. PERFORMING ORGANIZATION (If joint or other than NBS, see instructions)

NATIONAL BUREAU OF STANDARDS
DEPARTMENT OF COMMERCE
WASHINGTON, D.C. 20234

7. Contract/Grant No.

8. Type of Report & Period Covered

9. SPONSORING ORGANIZATION NAME AND COMPLETE ADDRESS (Street, City, State, ZIP)

U.S. Army Belvoir RD&E Center
Ft. Belvoir, VA 22060

10. SUPPLEMENTARY NOTES

☐ Document describes a computer program; SF-185, FIPS Software Summary, is attached.

11. ABSTRACT (A 200-word or less factual summary of most significant information. If document includes a significant bibliography or literature survey, mention it here)

Clutter models for subsurface electromagnetic applications are discussed with emphasis on tunnel detection applications. Random medium models are more versatile and require less detailed information than deterministic models. The Born approximation is used to derive expressions for the incoherent field, and electric and magnetic dipoles are treated in detail. When random inhomogeneities are located in the near field of the dipole source, an electric dipole radiates a larger incoherent field than a magnetic dipole because of its larger reactive electric field.

12. KEY WORDS (Six to twelve entries; alphabetical order; capitalize only proper names; and separate key words by semicolons)

clutter; coherent field; electric dipole; incoherent field; magnetic dipole; random medium

13. AVAILABILITY

☒ Unlimited

☐ For Official Distribution. Do Not Release to NTIS

☐ Order From Superintendent of Documents, U.S. Government Printing Office, Washington, D.C. 20402.

☒ Order From National Technical Information Service (NTIS), Springfield, VA. 22161

14. NO. OF PRINTED PAGES

48

15. Price

USCOMM-DC 6043-P80

*-U.-S.- GOVERNMENT PRINTING OFFICE: 1989 -674-724/ 5048